

A Geometry-based Stochastic Wireless Channel Model using Channel Images

Seongjoon Kang
NYU Wireless, Brooklyn, NY, USA
Email: sk8053@nyu.edu

Abstract—Due to the high complexity of geometry-deterministic wireless channel modeling and the difficulty in its implementation, geometry-based stochastic channel modeling (GSCM) approaches have been used to evaluate wireless systems. This paper introduces a new method to model any GSCM by training a generative neural network using images formed by channel parameters. In this work, we obtain channel parameters from the ray-tracing simulation in a specific area and process them in the form of images to train any generative model. Through a case study, we confirm that the use of channel images completes the training of the generative model within 10 epochs. In addition, we show that the trained generative model based on channel images faithfully represents the distributions of the original data under the assigned conditions. Therefore, we argue that the proposed data-to-image methods will facilitate the modeling of GSCM using any generative neural network under general wireless conditions.

Index Terms—generative AI - based channel modeling, generative neural networks, ray-tracing, channel images, GSCM, GAN

I. INTRODUCTION

The goal of communication channel modeling is to facilitate link- and system-level simulations in which the performance of the wireless system is evaluated. The 3rd Generation Partnership Project (3GPP) proposes different types of stochastic channel model depending on wireless systems such as aerial and satellite communications for benchmarking [1]–[3].

The statistical channel models proposed by 3GPP aim at general scenarios such as urban micro- and rural regions and do not take into account geometry-specific scenarios. To consider geometry-specific scenarios, deterministic models such as using ray-tracing simulation are proposed on the basis of fundamental electromagnetic wave propagation theory. However, due to the higher running and implementation cost of the deterministic equivalent, geometry-based stochastic channel modeling (GSCM) is proposed [4], which models the channel parameters through statistical distributions of predefined local scatters in certain environments.

To simplify GSCM, data-driven generative neural networks are used [5]–[10]. However, prior efforts to model GSCM require the high complexities of implementation and do not generalize the modeling for any wireless condition. For example, the authors of [7] propose a variational autoencoder (VAE) to capture the channel parameter statistics. This work requires two-step procedures—link classifier and VAE—to generate channel parameters. Following the same implementation pro-

cedures, in [8], the cluster generative model is proposed using Wasserstein generative adversarial networks with gradient penalty (WGAN-GP). However, this effort has pronounced shortcomings in the aspect of simulation accuracy, as more multipath components need to be observed in a wideband due to the higher time resolution.

Therefore, it is desirable to simplify and generalize the implementation of GSCM using any generative model to capture the statistics of the parameters of multipath channels, such as path loss, propagation delay, and arrival and departure angles. In this work, we propose methods to convert the parameters of wireless channels to certain types of images, which we define as *channel images*, and argue that newly generated channel images facilitate training of the given generative model and reduce the complexity of implementation. In addition, via a case study, we show that the output values from the trained model are statistically well matched to those from the original data.

II. CHANNEL IMAGE GENERATION

In this section, we discuss the proposed methods for processing and creating images from raw data on channel parameters before training a generative model. Since measuring realistic wireless channels in any region is challenging, we run the ray-tracing simulator and obtain the data from it.

A. Channel Parameters from Ray-tracing Simulation

The parameters of the wireless channel for a specific region are obtained from the commercial ray tracer, Wireless Insite [11]. For each link i between a transmitter and receiver, the channel parameter matrix $\mathbf{D}^i \in \mathbf{R}^{8 \times N}$ obtained from the ray tracing simulator is represented in the following way:

$$\mathbf{D}^i = \begin{pmatrix} pl_1 & pl_2 & \dots & pl_N \\ dly_1 & dly_2 & \dots & dly_N \\ aod_1 & aod_2 & \dots & aod_N \\ zod_1 & zod_2 & \dots & zod_N \\ aoa_1 & aoa_2 & \dots & aoa_N \\ zoa_1 & zoa_2 & \dots & zoa_N \\ ps_1 & ps_2 & \dots & ps_N \\ ls_1 & ls_1 & \dots & ls_1 \end{pmatrix} \quad (1)$$

where N is the total number of multipaths, pl is pathloss, dly is propagation delay, aod and zod are azimuth and zenith angles of departure (AOD and ZOD), aoa and zoa are azimuth and zenith angles of arrival (AOA and ZOA), ps is the arrival

phase at receiver side, and ls_1 is the link state of the first arrival path. Note that we only need the link state of the first arrival path since the other paths are non-line-of-site (NLOS) paths. The single matrix representation for all channel parameters on one link becomes useful in building channel images.

For line-of-site (LOS) path, the path components, such as pathloss, delay, and angles, are computed mathematically as the following:

$$pl_1 = 20 \log_{10}(\text{dist}_{3d}) + 20 \log_{10}(f) - 147.55 \quad (2a)$$

$$dly_1 = \frac{\text{dist}_{3d}}{c} \quad (2b)$$

$$aod_1 = \arctan \frac{y_{tx} - y_{rx}}{x_{tx} - x_{rx}} \quad (2c)$$

$$aoa_1 = aod_1 - 180 \quad (2d)$$

$$zod_1 = \arctan \frac{\text{dist}_{2d}}{z_{rx} - z_{tx}} \quad (2e)$$

$$z oa_1 = 180 - zod_1 \quad (2f)$$

$$ps_1 = -360(f \cdot dly_1 - \lfloor f \cdot dly_1 \rfloor) \quad (2g)$$

where dist_{3d} is 3D distance between a transmitter and a receiver, f is the carrier frequency, c is the speed of light, (x_{tx}, y_{tx}) and (x_{rx}, y_{rx}) are the 2D coordinates of the transmitter and the receiver. Thus, the LOS parameters are obtained deterministically by Eqs. 2a - 2g. However, for the NLOS path, we should rely on the results of the ray-tracing simulator, since NLOS components are related to the network environments in which the transmitters and receivers are located.

B. Data Normalization

In order to use a generative neural network, the raw data obtained by the ray-tracing simulation are normalized by employing *Min-Max* scaling to make all elements of the data matrix $\mathbf{D}^i \in \mathbf{R}$ in the range of -1 to 1. The pre-processing of raw data is a common method to reduce the variances of data. Suppose that the M transmitter-receiver links are simulated in ray-tracing simulation. Since each link has a different number of paths, the corresponding data matrices \mathbf{D} have different data shapes. To make the size of the data matrix the same across all links, we introduce the *virtual paths* when the number of paths is less than the maximum number of paths, which is 25 in this work. Except the pathloss feature, the virtual values for the feature data d_i are sampled from the uniform distribution $U(\min d_i, \max d_i)$. For the pathloss feature, we choose virtual values that are higher than the maximum pathloss value—180 dB, since the pathloss values will become the main criteria for distinguishing virtual and real paths. In this way, we make the dimension of every data matrix \mathbf{D}^i the same and define the total data tensor $\mathbf{D} = \{\mathbf{D}^1, \mathbf{D}^2, \dots, \mathbf{D}^M\} \in \mathbf{R}^{M \times 8 \times 25}$.

Before Min-Max scaling of raw data, for each link i , we take into account the following additional data processing technique for some feature data.

- Pathloss: Since we assume that the transmitter and receiver locations are known, we normalize the pathloss

values of each path by the free space pathloss (FSPL) using Eq. 2a

$$\tilde{pl} = pl - FSPL(\text{dist}_{3d})$$

- Delay: Similarly, the delay values are normalized by the LOS delay using Eq. 2b

$$\tilde{dly} = dly - \frac{\text{dist}_{3d}}{c}$$

Considering that delay values are relatively small compared to other feature data, we multiply them by a sufficiently large scalar value— 10^7 .

- Link state: To take into account the link state of the first arrival path, for a very small value ϵ ($0 < \epsilon \ll 1$), the link state values are sampled from uniform distributions, which are $U(1 - \epsilon, 1)$ for LOS and $U(-1, -1 + \epsilon)$ for NLOS, respectively.

We do not consider angles relative to the LOS directions because this processing might not be invertible under certain conditions. For example, when the conditional variables are the 2D distance between a transmitter and receiver and the height of a receiver, the AOD and AOA are not recoverable from angles relative LOS directions.

The Min-Max scaling for each feature data is given as the following:

$$\hat{d}_i = \frac{(2 \times d_i - \max d_i - \min d_i)}{\max d_i - \min d_i}$$

$$d_i = \mathbf{D}_{:,i,:}$$

Note that all the pre-process for raw data must be invertible, since we need the inverse process to recover data from the output of the generative model.

C. Data-to-Image Mapping

After pre-processing the data, we create channel images corresponding to each wireless connection between a transmitter

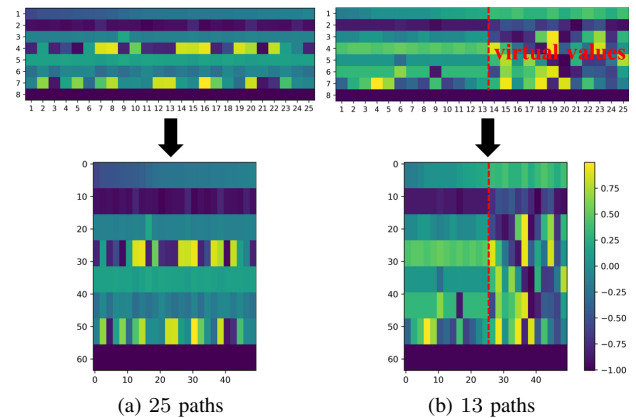


Fig. 1: Images for different number of multipaths are generated by zooming in the matrices of pre-processed channel parameters.

and receiver. The formation of images is instrumental because deep convolutional generative networks can easily perform edge detections and capture correlations between pixels in the images. In this work, we simply enlarge the data matrix D^i by repeating each element of the matrix horizontally and vertically.

We replicate each element of the data matrix $D^i \in \mathbf{R}^{8 \times 25}$ by 2 times horizontally and 8 times vertically, and thus the size of the resulting matrix becomes $\tilde{D}^i \in \mathbf{R}^{64 \times 50}$. Fig. 1 shows the process of creating images from the original data matrices for two different multipath cases. As shown in Fig. 1b, when the number of multipaths is less than 25, the virtual values are filled to make the size of the data matrix consistent.

III. DESIGN OF CONDITIONAL GENERATIVE MODEL

The main goal of GSCM in this work is to capture channel statistics for a specific region under certain conditions, such as receiver heights, distances between the transmitter and the receiver, and carrier frequencies. Therefore, we need to design a generative model that can conditionally output the channel parameters.

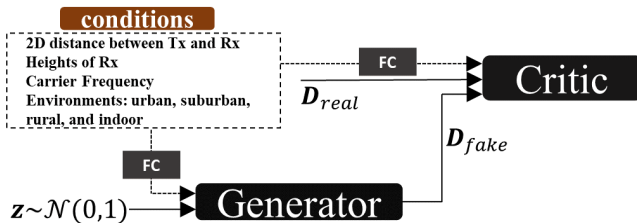


Fig. 2: WGAN-GP with general wireless conditions

As one example of the conditional generative model, we employ WGAN-GP [12]. For more detailed descriptions of WGAN and WGAN-GP, we refer to [12], [13]. Fig. 2 shows the structure of WGAN-GP with general wireless conditions, such as 2D distances, heights, carrier frequencies, and network environments, which can be embedded both of the generator and critic, respectively, through fully connected neural networks (FC), as shown in Fig. 2. The hyper-parameters for training are listed in Table I, and the structure of our WGAN-GP is similar to [12]. All detailed implementations are uploaded in [14].

TABLE I: Hyper-parameters to train WGAN-GP

	Generator	Critic
Input image size	[64, 50, 1]	
Learning rate	5×10^{-5}	
Optimizer	Adam ($\beta_1 = 0.5, \beta_2 = 0.9$)	
Epochs	10	
Batch size	256	
Number of parameters	4,074,726	4,016,597

IV. CASE STUDY AND RAY-TRACING SIMULATION

In this section, we discuss the case study on GSCM with conditional constraints and explain the ray-tracing simulation

to obtain the wireless channel parameters in the given region. Note that the main assumption throughout this work is that the transmitter and receiver locations are known.

A. Case Study: Different Receiver Heights

In this study, we want to capture the statistical distribution of local scatters at different 2D distances between transmitters and receivers. In addition, we take into account different receiver heights with fixed carrier frequency. Thus, the learning process of the statistical distribution of the data matrix D can be described as follows:

$$P(D|\text{dist2d}, h) = P(T\mathcal{G}(\text{dist2d}, h)) \quad (3)$$

where \mathcal{G} is any conditional generative model—WGAN-GP in our work, and T is an operator to perform image-to-data mapping process, i.e., the process from outputs of the model to the original data matrix D . Note that we can add more conditional variables with the functions of 2D distance dist2d and height h , e.g., 3D distances and zenith angles. The five discrete receiver heights, 1.6 m, 30 m, 60 m, and 120 m, are considered to model terrestrial and aerial channels simultaneously. The 2D distances obtained from all the transmitter and receiver pairs are continuous values in the range of the network area.

B. Ray-tracing Simulation

To secure channel parameter data for the aforementioned case study, we run a ray-tracing simulation in Herald Square in New New York City, which can be considered a typical dense urban area. We select the upper mid-band carrier frequency 12 GHz, which is recognized as the promising spectrum in future networks [15], [16], and all electrical properties, such as permeability and conductivity, corresponding to 12 GHz, are set for each material. The data from this ray-tracing simulation can be used to model integrated aerial-terrestrial wireless channels.

Fig. 3 shows the area, Herald Square in New York City, for the ray-tracing simulation where transmitters are placed on top of buildings and receivers are dropped on the outdoor



Fig. 3: Herald Square in New York city for ray-tracing simulation. (1120 m \times 510 m). The green rectangles represent transmitters, and the yellow rectangles are receivers.

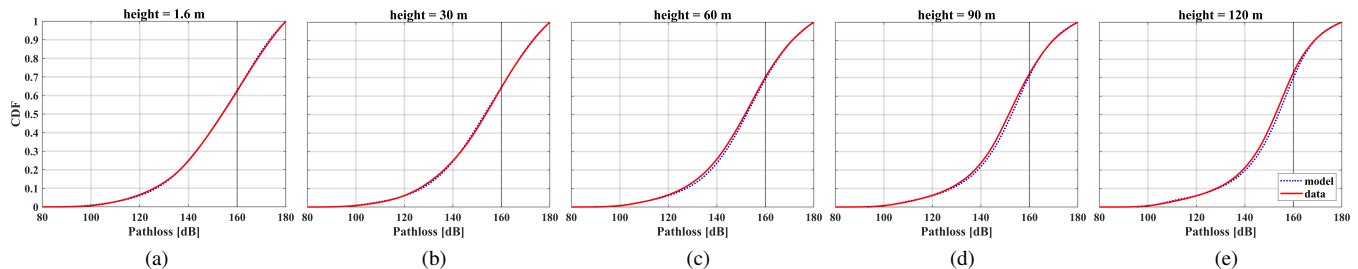


Fig. 4: CDFs of pathloss for (a) 1.6 m, (b) 30 m, (c) 60 m, (d) 90 m, and (e) 120 m

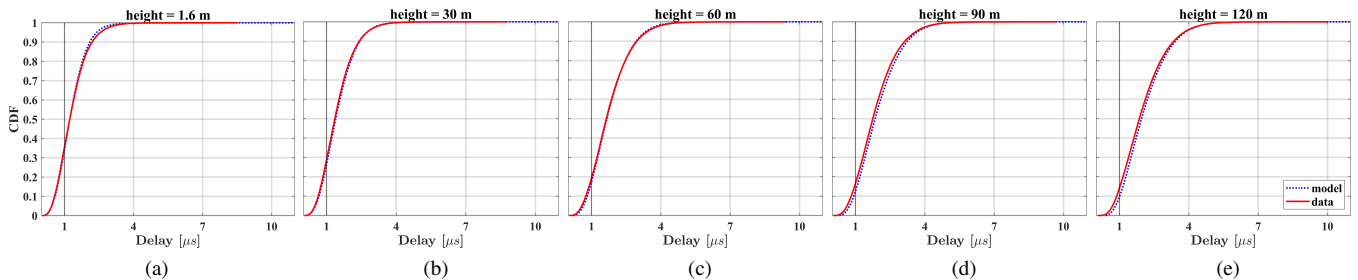


Fig. 5: CDFs of propagation delay for (a) 1.6 m, (b) 30 m, (c) 60 m, (d) 90 m, and (e) 120 m

street randomly. In Fig. 3, different colors indicate different materials. For example, gray is concrete, light blue is glass, and brown is brick. To capture transmitted rays in all directions, transmitters and receivers are equipped with the single *isotropic* antennas. In this simulation, we deploy 79 transmitters on top of buildings and 1526 outdoor receivers for five different heights: 1.6, 30, 60, 90, 120 m. Thus, in total $79 \times 5 \times 1526 = 602,770$ links are obtained.

V. DATA RECOVERING PROCESS

We confirmed that within 10 epochs of training, the channel images generated from the model become similar to the original. After the train, the output matrices $\tilde{D}_{\text{image}} \in \mathbf{R}^{64 \times 50}$ of WGAN-GP are processed reversely following all the steps described in Section II.

First, the size of the output matrices should be decreased using a suitable sampling method: $\tilde{D}_{\text{image}} \in \mathbf{R}^{64 \times 50} \rightarrow \tilde{D} \in \mathbf{R}^{8 \times 25}$. After reducing the size of the model output, all data are recovered by the *reverse* Min-Max scaling. In particular, to recover pathloss and delay values, FSPL and minimum delay values calculated using Eqs. 2a and 2b are added to pathloss and delay values after reverse Min-Max scaling. To determine the state of the link, we take the average in the last row of the output matrix \tilde{D} . If the average value is positive, the link state is LOS and, otherwise, NLOS.

Once a link state is determined as LOS, all channel parameters corresponding to the first arrival path are deterministic. Thus, when the link state value from \tilde{D} indicates the LOS state, the first column of the data matrix \tilde{D} is replaced with the channel parameters calculated by Eqs. 2a- 2g using the transmitter and receiver coordinates. Finally, virtual paths are

discerned and removed when pathloss values are larger than the outage value 180 dB.

VI. EVALUATION ON TRAINED MODEL

To evaluate the quality of the channel statistics captured by WGAN-GP, we analyze the output statistics from our model by comparing them with the original data.

Fig. 4 shows the cumulative distribution functions (CDF) of pathloss on all paths over all links. We observe that the CDFs drawn by the data from the model are aligned with the CDFs by the original data. In particular, the conditionality by heights holds, as we confirm that the probability of $pl > 160$ dB decreases at higher altitudes in Fig. 4. Similarly, as shown in Fig. 5, we observe that two CDFs (model and data) of propagation delays on all paths of all links are well matched. In addition, at each height, we see the different conditional distributions, since the probability of $dly < 1\mu s$ decreases at higher altitudes. This is mainly because in dense urban areas, the NLOS propagation paths are dominant when the receiver heights are lower.

Fig. 6 shows the probabilities of LOS and link failure at different 2D distances. We define a communication link outage if all pathloss values of a multipath are greater than 180 dB. At higher altitudes, the receivers are more visible to the transmitters. Therefore, the probability of LOS is higher at higher altitudes, whereas the probability of outage is lower. We observe that the link state probabilities (LOS and outage) at each height obtained from our model are well matched with the probabilities calculated with the original data. This result implies that the trained model holds two conditional constraints well, 2D distances and heights.

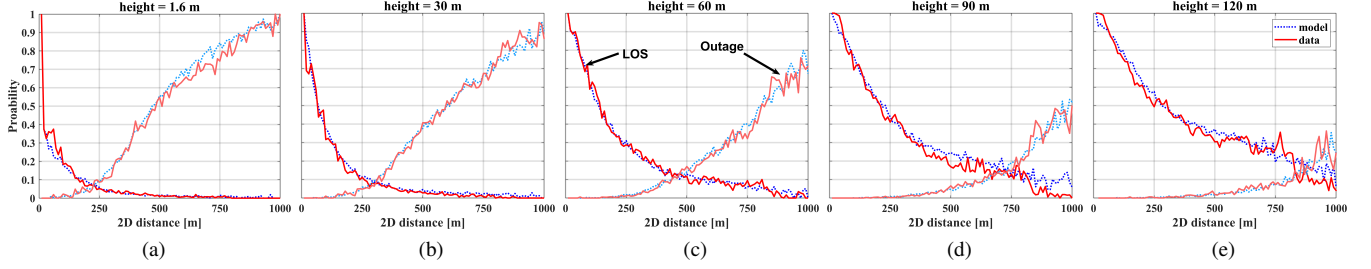


Fig. 6: Link state probability (LOS and outage) for (a) 1.6 m, (b) 30 m, (c) 60 m, (d) 90 m, and (e) 120 m

To compare the angular distributions between our model and the original data, we took into account the angles relative to the LOS directions. In this case, we can only evaluate the statistics of the ZOD and ZOA under the conditions of 2D distances and heights. We define a random variable, a relative angle to the LOS direction, simply by subtracting the ZOD and ZOA of the LOS, which can be computed using Eq. 2e and 2f. Consequently, the probability density function (PDF) for the relative angle of ZOD conditioned with 2D distance dist_{2D} and height h is described as follows:

$$P(zod(\text{dist}_{2D}, h) - zod_{LOS}(\text{dist}_{2D}, h)) = P\left(zod(\text{dist}_{2D}, h) - \arctan\left(\frac{\text{dist}_{2D}}{h}\right)\right) \quad (4)$$

In the same way, we define the PDF of ZOAs relative to LOS direction using Eq. 2f.

Fig. 7 depicts the PDFs of ZOA and ZOD as heatmaps obtained from the original data and outputs of our model at different receiver heights. Each column in the heatmaps represents the PDF calculated at the corresponding 2D distance. On the one hand, as the 2D distances increase, we observe that ZOA and ZOD have less angular spread as a result of less scattering at a far distance. On the other hand, since the local scattering increases at a closer distance, we see a large variation of the relative angles until 200 m of the 2D distance.

Specifically, local scatterings occur mostly in downward directions at close distances. Accordingly, Fig. 7a and Fig. 7b illustrate the following interesting results:

- On the transmitter side, we can easily confirm that the LOS ZOD decreases as the receiver height increases. As shown in Fig. 7a, at 1.6 m altitude, we observe a higher probability at negative relative angles (LOS ZODs > ZODs). On the contrary, at 120 m altitude, positive relative angles (ZODs > LOS ZODs) have a higher probability as the LOS ZODs decrease.
- On the receiver side, as opposed to the transmitter case, the LOS ZOA increases as the receiver height increases. Therefore, in Fig. 7b, the positive relative angles (ZOAs > LOS ZOAs) have higher probabilities at 1.6 m altitude, while at 120 m altitude, the probability of negative relative angles (LOS ZOAs > ZOAs) is higher.

Since the conditional variables are 2D distances and heights, azimuth angles (AOA, AOD) and arrival phases follow the

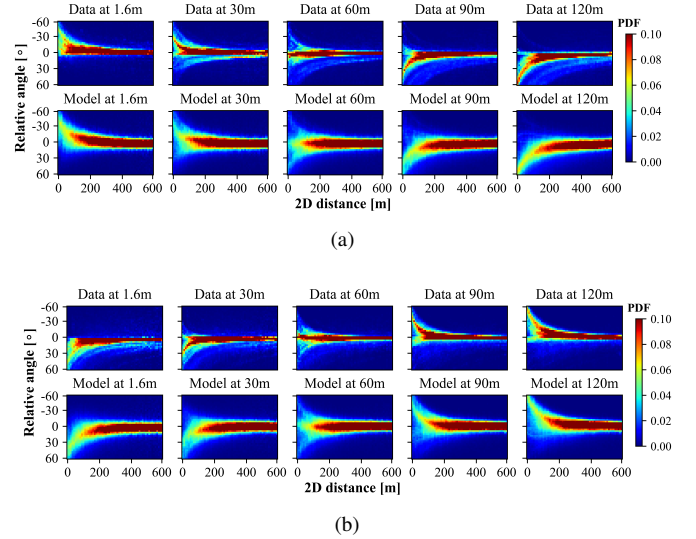


Fig. 7: PDFs of relative (a) ZOD and (b) ZOA over 2D distances

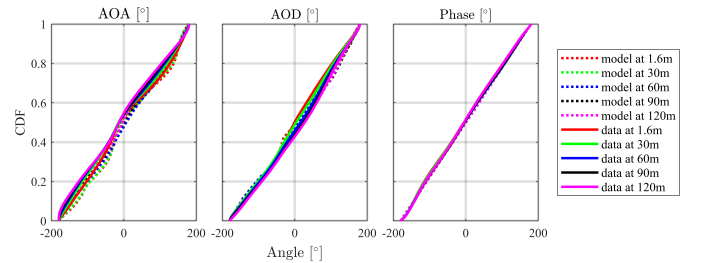


Fig. 8: CDFs of AOA, AOD and arrival phase

uniform distribution. Note that for AOA and AOD statistics, Eq. 4 is not available and, therefore, it is not possible to show heatmaps of PDFs such as Fig. 7a and Fig. 7b. In other words, to calculate LOS azimuth angles, Eq. 2c is not available due to

$$P(aod|\text{dist}_{2D}, h) \neq P(aod|dx, dy, h)$$

where $dx = x_{rx} - x_{tx}$ and $dy = y_{rx} - y_{tx}$.

As shown in Fig. 8, the distributions of AOA, AOD, and arrival phase are uniform at each height owing to the conditionality of the 2D distance.

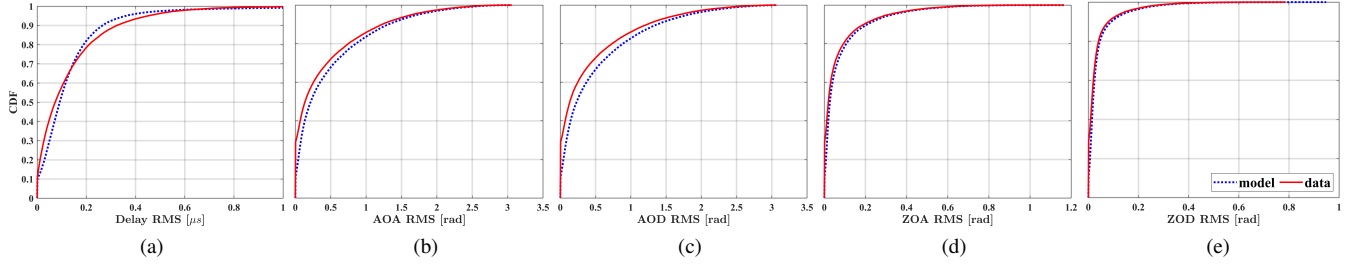


Fig. 9: RMS CDFs for (a) delay, (b) AOA, (c) AOD, (d) ZOA, and (e) ZOD

As the last evaluation of the model, we briefly discuss the root mean square (RMS) spread for the delay, azimuth, and zenith angles, which represents the degree of sparsity or richness of the multipath channels. According to [17], the general RMS spread values for a multipath feature \mathbf{d} are calculated as follows:

$$d_{rms} = \sqrt{\frac{\sum_k (d_k - d_m)^2 P_k}{\sum_k P_k}}, \quad d_m = \frac{\sum_k d_k P_k}{\sum_k P_k}$$

where P_k is path gain, d_k is channel parameters such as *excess delay*, arrival and departure angles at k 'th path. RMS values are an instrumental metric in dense urban environments where there are many local scatters. We consider the RMS values of delay, AOA, AOD, ZOA and ZOD when the receiver height is 1.6 m, as at lower altitude rich scatterings can occur. The statistical distributions of the RMS values are shown in Fig. 9 as CDF for AOA, AOD, ZOA, ZOD and delay. As shown, we observe that the distributions are very closely aligned with those of the original data. These results imply that the WGAN-GP statistically well captures the multipath characteristics that reflect rich or sparse scatterings.

VII. CONCLUSION

In this work, we introduce a simplified method for building GSCM given specific conditional constraints based on channel parameter data obtained from ray-tracing simulation. Because building a theoretical GSCM that captures all the statistics of local scatters is very challenging, generative neural networks are considered. Specifically, WGAN-GP is adopted in this paper. We propose methods to convert all channel parameters to images to reduce the complexity of WGAN-GP training and implementation. After training the model, we confirm that the statistics of all the channel parameters of WGAN-GP are well matched with the distributions of the original data.

Thus, we argue that given wireless channel data from any geometry or a specific site, generative models can be leveraged with the proposed channel image methods for GSCM. Depending on the accuracy constraints of modeling and implementation complexities, other generative models, such as VAE and the diffusion models, can be employed. Finally, using the proposed channel images, other wireless

conditions, such as multi-carrier frequencies and different scenarios of environments, will be readily implemented to assess and compare the network performances.

REFERENCES

- [1] 3GPP, "TR 38.901, 5G; study on channel model for frequencies from 0.5 to 100ghz," 2017.
- [2] —, "TR 36.777, 3rd generation partnership project; technical specification group radio access network; study on enhanced lte support for aerial vehicles," 2017.
- [3] —, "TR 38.811, 3rd generation partnership project; technical specification group radio access network; study on new radio (nr) to support non-terrestrial networks," 2020.
- [4] X. Yin and X. Cheng, *Propagation channel characterization, parameter estimation, and modeling for wireless communications*. John Wiley & Sons, 2016.
- [5] Y. Yang, Y. Li, W. Zhang, F. Qin, P. Zhu, and C.-X. Wang, "Generative-adversarial-network-based wireless channel modeling: Challenges and opportunities," *IEEE Communications Magazine*, vol. 57, no. 3, pp. 22–27, 2019.
- [6] T. Orekondy, A. Behboodi, and J. B. Soriaga, "Mimo-gan: Generative mimo channel modeling," in *ICC 2022-IEEE International Conference on Communications*. IEEE, 2022, pp. 5322–5328.
- [7] W. Xia, S. Rangan, M. Mezzavilla, A. Lozano, G. Geraci, V. Semkin, and G. Loianno, "Generative neural network channel modeling for millimeter-wave uav communication," *IEEE Transactions on Wireless Communications*, 2022.
- [8] Y. Hu, M. Yin, W. Xia, S. Rangan, and M. Mezzavilla, "Multi-frequency channel modeling for millimeter wave and thz wireless communication via generative adversarial networks," *arXiv preprint arXiv:2212.11858*, 2022.
- [9] H. Xiao, W. Tian, W. Liu, and J. Shen, "Channelgan: Deep learning-based channel modeling and generating," *IEEE Wireless Communications Letters*, vol. 11, no. 3, pp. 650–654, 2022.
- [10] S. Seyedsalehi, V. Pourahmadi, H. Sheikhzadeh, and A. H. G. Fomani, "Propagation channel modeling by deep learning techniques," *arXiv preprint arXiv:1908.06767*, 2019.
- [11] "Remcomm [online]," <https://www.remcom.com>, online; accessed 28 November 2022.
- [12] I. Gulrajani, F. Ahmed, M. Arjovsky, V. Dumoulin, and A. C. Courville, "Improved training of wasserstein gans," *Advances in neural information processing systems*, vol. 30, 2017.
- [13] M. Arjovsky, S. Chintala, and L. Bottou, "Wasserstein generative adversarial networks," in *International conference on machine learning*. PMLR, 2017, pp. 214–223.
- [14] "Geometry-based stochastic wireless channel modeling git hub repository," available on-line at <https://github.com/sk8053/GeoStochasticChanModel>.
- [15] FCC Technical Advisory Council, "FCC seeks comment on maximizing efficient use of 12 GHz band," January 2021. [Online]. Available: <https://www.fcc.gov/document/fcc-seeks-comment-maximizing-efficient-use-12-ghz-band>
- [16] —, "6G working group position paper," August 2023. [Online]. Available: https://www.fcc.gov/sites/default/files/Consolidated_6G_Paper_FCCTAC23_Final_for_Web.pdf

[17] ITU-R P.1407-6, "Multipath propagation and parameterization of its characteristics," Jun 2017.